Probing Heterogeneity in Attenuated Total Reflection Surface-Enhanced Infrared Absorption Spectroscopy (ATR-SEIRAS) Response with Synchrotron Infrared Microspectroscopy

Kaiyang Tu[1,2], Tyler A. Morhart[1,2], Stuart T. Read[2],
Scott M. Rosendahl[2] , and Ian J. Burgess[1]

Abstract

The heterogeneity of metal island films electrodeposited on conductive metal oxide modified internal reflection elements is shown to provide a variable attenuated total reflection surface-enhanced infrared absorption spectroscopy (ATR-SEIRAS) response. A self-assembled monolayer of a ferrocene-terminated thiol monolayer ($FcC_{11}SH$) was formed on the gold islands covering a single substrate, which was measured using both a conventional spectrometer and a custom-built horizontal microscope. Cyclic voltammetry and ATR-SEIRAS results reveal that the $FcC_{11}SH$-modified substrate undergoes a reversible electron transfer and an associated re-orientation of both the ferrocene/ferrocenium headgroup and the hydrocarbon backbone. The magnitude of the absorption signal arising from the redox changes in the monolayer, as well as the IR signature arising from the ingress/egress of the perchlorate counterions, is shown to depend significantly on the size of the infrared beam spot when using a conventional Fourier transform infrared spectrometer. By performing equivalent measurements on a horizontal microscope, the primary cause of the differences in the signal level is found to be the heterogeneity in the density of gold islands on the conductive metal oxide.

Introduction

Surface heterogeneity plays an important, but often hard to assess, role in many chemical and physical processes occurring at electrochemical interfaces. The operative length scales where surface heterogeneity influences catalytic reactions spans from atomic to microscopic dimensions.[1] Much work has focused on the influence of nanometer length-scale surface structure, such as localized crystallographic domains, in electrocatalysis.[2] On a more microscale dimension, the influence of grain boundaries and polydispersity in metal texturing complicates the detected analytical signal in electrochemical biosensor interfaces.[3] Product selectivity depends on interparticle separation and catalyst loading density in many important reactions such as the reductions of molecular oxygen[4,5] and carbon dioxide.[6] Consequently, distributions in the size and average particle separation can lead to inhomogeneous reactant and product distributions in functioning fuel cells and electrolyzers.

Spectroscopy, particularly microspectroscopy, is an important tool for mapping heterogeneity in electrocatalyst activity and selectivity.[7] The high molecular sensitivity and (sub)monolayer detection limits of surface sensitive infrared methods make them particularly powerful for in situ studies of electroactive interfaces. Attenuated total reflection

[1]Department of Chemistry, University of Saskatchewan, Saskatchewan, Canada
[2]Canadian Light Source, Saskatoon, Canada

Corresponding author:
Ian J. Burgess, Department of Chemistry / Thorvaldson Building, University of Saskatchewan, Saskatoon, Saskatchewan S7N5C9, Canada.
Email: ian.burgess@usask.ca

surface-enhanced infrared absorption spectroscopy (ATR-SEIRAS) is well suited for studying electrocatalysis reactions due to the generation of highly localized electric fields around metal nanoparticles leading to excellent surface sensitivity and a lack of interference from the bulk electrolyte.[8] The surface enhancement effect in ATR-SEIRAS is present in non-coinage metals making the technique applicable to highly electrocatalytically active metals such as Pt,[9] Rh,[10] and Pd,[11,12] as well as first row transition metals.[13] However, in general, the spatial resolution of surface sensitive infrared spectroscopy is diffraction limited unless coupled with near-field techniques that, with few exceptions,[14,15] are incompatible with in situ/operando electrochemical conditions. This has greatly limited the use of infrared-based techniques for spectroelectrochemical mapping experiments.[16,17] Nevertheless, the development of a robust platform suitable for ATR-SEIRAS mapping of electrocatalytic systems is an appealing proposition. We have recently advocated the use of thin films of conductive metal oxide (CMO) as the supporting layer in electrochemical ATR-SEIRAS experiments.[18] Metal island films can be directly electrodeposited on these surfaces and the resulting metal-island modified surfaces have been shown to give larger enhancement factors than traditional metal films grown directly on infrared prisms. These metal@CMO films are often quite heterogeneous in appearance, and the electrodeposited nanoparticles are unequally distributed on the conductive metal oxide surface. In the present study, we have coupled an Au@ITO (indium tin oxide) SEIRAS substrate with synchrotron infrared radiation (SIR) to demonstrate the ability of a horizontal ATR microscope to map heterogeneity in a film of an electroactive self-assembled monolayer.

Experimental

Reagents

Used as received were NaF ($>99.98\%$, Aldrich), $KAuCl_4$, (98%, Aldrich) and 4-methoxypyridine (MOP) (97%, Aldrich), KCl (ACS grade, Fisher Scientific). Potassium perchlorate (ACS grade, Fisher Scientific) was recrystallized. 11-(Ferrocenyl)undecanethiol ($FcC_{11}SH$) was kindly synthesized and purified as reported previously[19] and supplied by Antonella Badia (Université de Montréal). All aqueous solutions were made using Milli-Q water ($>18.1\,M\Omega\bullet cm$).

Au@ITO Layer Preparation and $FcC_{11}SH$ SAM Incubation

The SEIRAS-active Au@ITO layers were prepared following a previously reported procedure[18] with minor modifications. A 25 nm thick indium tin oxide film (ITO) was deposited onto a microgrooved Si internal reflection element (IRE) (Si μ-groove IRE, IRUBIS GmbH) using a home-built RF magnetron sputtering unit. The ITO target (Kurt J. Lesker) was composed of 90% In_2O_3 and 10% SnO_2 by weight. Sputtering was conducted at 30 W power and a base pressure of 2×10^{-5} Torr. Freshly sputtered ITO films were subsequently annealed at 300 °C in vacuum for 1 h.[20] The annealed ITO-modified Si wafer was assembled in a custom-built spectroelectrochemical cell holding 0.1 M NaF solution and subsequently purged with Argon for 20 min; 250 μM $KAuCl_4$ and 100 μM MOP were added to the solution, followed immediately by electrodeposition of Au. Starting at the open-circuit potential, a 20 mV/s voltammetric sweep was applied to the ITO working electrode between −1.0 V and +1.0 V for three cycles. Subsequent ATR-SEIRAS measurement of MOP adsorption and desorption on Au at +300 mV and −900 mV, respectively, provided a spectroscopic handle on the infrared (IR) activity of the electrodeposited Au layer. Similar electrodeposition steps were applied to increase the SEIRAS-activity until the MOP IR signature plateaued. The freshly prepared Au@ITO-modified μ-groove wafer was removed from the cell and thoroughly rinsed with Milli-Q water followed by an ethanol rinse. The μ-groove wafer was then placed into an aluminum wrapped vial containing an ethanol solution of 0.1 mM $FcC_{11}SH$ for 6 h, followed by thorough rinsing with ethanol to remove physisorbed thiols and a subsequent rinse with Milli-Q water to remove residual ethanol. Once reassembled into the spectroelectrochemical cell, 0.1 M $KClO_4$ was added and the cell was purged with Argon for 20 min.

In Situ Spectroelectrochemistry

All electrochemical and spectroelectrochemical experiments were performed using a HEKA PG 590 potentiostat. Current and potential data were collected using a USB 6351 X-series multifunction digital to analogue converter (National Instruments) controlled through an in-house written LabView interface. The custom-built spectroelectrochemical cell consisted of a standard three electrode configuration with the Au@ITO film on the μ-groove IRE serving as the working electrode. The reference and counter electrodes were an Ag–AgCl wire in a saturated KCl solution (connected by a salt bridge) and a coiled gold wire, respectively, and the electrolyte solution was 50 mM $KClO_4$. A Bruker Vertex 70 Fourier Transform Infrared (FT-IR) spectrometer was used for non-synchrotron-based measurements. The assembled spectroelectrochemical cell fits a Pike Technologies VeeMAX III ATR accessory set to a 55° angle of incidence. Synchrotron IR-based measurements utilized a Bruker Vertex 70v FT-IR spectrometer. All FT-IR spectra were derived from 512 individual scans with 8 cm^{-1} wavenumber resolution. Spectra are reported formally as changes in absorbance as defined by $Abs = -\log(S_{E_{sample}}/S_{E_{ref}})$, where $S_{E_{sample}}$ and $S_{E_{ref}}$ are the

single beam spectra recorded at the sample and reference potentials, respectively.

Results and Discussion

FcC$_{11}$SH Monolayer Electrochemistry

A freshly prepared FcC$_{11}$SH SAM on an Au@ITO-modified IRE substrate was assembled in the spectroelectrochemical cell and electrochemically characterized using cyclic voltammetry (CV) in 0.1 M KClO$_4$ electrolyte (Fig. 1). The region of potential stability of the FcC$_{11}$SH is delimited by the reduction and oxidation of the gold-thiolate bond in the SAM layer and depends on the number of hydrocarbons in the alkyl chain, the degree of order in the SAM, and the surface crystallography of the gold.[21] The Fc redox is considerably removed from the reductive desorption of the thiol which overlaps with hydrogen evolution in pH 6 electrolyte. Oxidative desorption occurs at potentials positive of "bare" gold surface oxidation,[22] which begins at about +0.80 V versus Ag/AgCl for polycrystalline gold. The large redox feature associated with the heterogeneous one electron redox of tethered ferrocene exhibits a formal potential, $E°$, of +0.398 V versus Ag/AgCl[23,24] and has a peak separation of about 25 mV. A smaller, but distinctive, shoulder is also observed at $\sim$ +0.30 V. Fitting the peaks in the CV to Gaussian functions reveals that the full width half-maximum (FWHM) of the principal peak is 95 mV. An ideal redox SAM (i.e., a system with kinetically fast electron transfer and no intermolecular interactions between neighbouring redox centres) should provide a single redox peak with a full-width half maximum of 90.6 mV and exhibit no potential separation between oxidation and reduction peaks.[25] Non-ideal behaviour in Fc terminated SAMs has
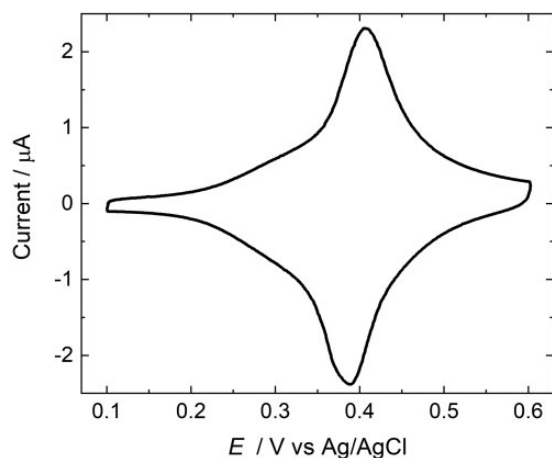

Figure 1. Cyclic voltammogram of the FcC$_{11}$SH SAM formed on the Au@ITO-modified internal reflection element in the spectroelectrochemical cell. Scan rate was 20 mV/s and the supporting electrolyte was 0.1 M KClO$_4$.

been extensively reported and traditional explanations invoke models of separate populations of the Fc terminus in the SAM.[19,23,24,26,27] Distinct domains of isolated ferrocene and clustered ferrocene are often cited as the source of multiple peaks when the SAM is formed from a binary mixture of a diluent thiol and a ferrocene terminated thiol.[23,28,29] In other reports, domains of ordered and disordered thiols were reported as the underpinning cause of the non-ideal electrochemical behaviour of ferrocene-terminated SAMs.[30–32] These models were recently challenged by Nerngchamnong et al.[26] who argued that multiple peaks and larger than expected FWHM were inherent to the mismatch in size between the Fc headgroup and the methylene units which causes a plurality of Fc microenvironments to release the buildup of strain in the monolayer. Irrespective of the underpinning physical explanation of the FcC$_{11}$SH electrochemistry, Fig. 1 reveals that the behaviour of the FcC$_{11}$SH SAM formed on the Au@ITO-modified IRE substrate is both thermodynamically and kinetically non-homogeneous. The coverage of FcC$_{11}$SH on the electrodeposited Au was estimated by integrating the CV. Using the geometrical surface area of the electrode exposed to the electrolyte multiplied by a roughness factor of $\sim$1.6[18] led to an estimated average coverage of 3.3×10^{-10} moles cm^{-2}. The value corresponds to an approximately 63% coverage of the Au when compared to the theoretical maximum coverage of FcC$_{11}$SH of 4.5×10^{-10} moles cm^{-2}.[31]

ATR-SEIRAS Characterization of FcC$_{11}$SH SAMs

ATR-SEIRAS spectra of the FcC$_{11}$SH SAM on Au@ITO were measured with a conventional IR configuration and a VeeMAX III ATR accessory as described elsewhere.[33] The IRE was a small ($\sim$10 mm $\times$ $\sim$10 mm $\times$ $\sim$0.5 mm), micromachined Si wafer (Si µ-groove IRE). The shorter pathlength through thin Si µ-groove IREs makes them considerably more transparent than traditional Si IREs (Si hemispheres or prisms with several cm pathlengths) and greatly increases optical throughput below $\sim$1400 cm^{-1}. Gold nanoparticles were electrodeposited on an ITO-coated Si µ-groove IRE and used as the working electrode in the ATR-SEIRAS studies. Potential-dependent spectra are shown in Fig. 2a with the single beam measurement at +0.10 V versus Ag/AgCl serving as the reference spectrum. The relative absorbance spectrum at +0.30 V contains only very weak peaks, consistent with the small contribution of the voltammetric shoulder, as shown in Fig. 1. The onset of ferrocene oxidation at potentials greater than +0.30 V corresponds to the appearance of several vibrational bands that increase in intensity with increasingly positive potential. Two positive absorbance peaks are observed at 3106 cm^{-1} and 1095 cm^{-1} and two peaks with negative absorbance changes are present at 2848 cm^{-1} and 2918 cm^{-1}. The latter two peaks are assigned to the methylene symmetric and asymmetric stretching modes respectively, whereas the
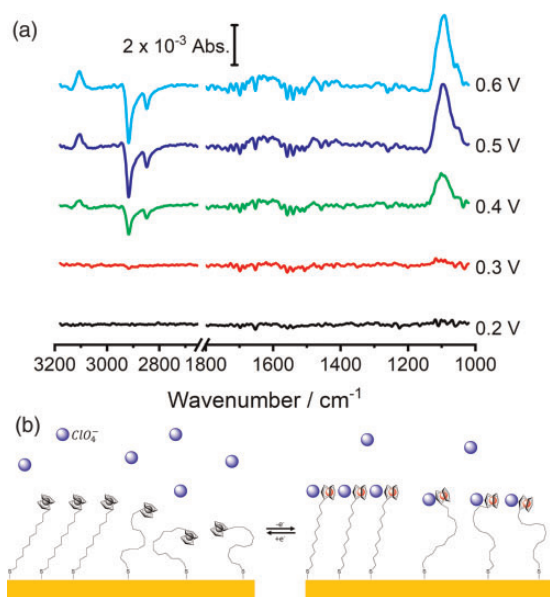
Figure 2. (a) Potential difference ATR-SEIRAS spectra of the FcC$_{11}$SH SAM formed on the Au@ITO-modified internal reflection element using a conventional ATR-SEIRAS configuration. The reference spectrum was collected at 0.1 V and the sample spectra were as indicated. (b) Schematic representation of the expected redox-induced orientation changes of FcC$_{11}$SH as adapted from Rudnev et al.[37]

Figure 3. Signal-to-noise asssesment of ATR-SEIRAS spectra of FcC$_{11}$SH using a conventional FT-IR spectrometer. (a) Potential-dependent spectra (E$_{ref}$ = 0.10 V, E$_{sample}$ = 0.60 V) as a function of the aperture diameter (b) measured noise dependence on

symmetric Cl–O stretch associated with the ingress of charge-compensating perchlorate anions gives rise to the signal at ∼1100 cm^{-1}.[34] Significantly weaker peaks arising from the methylene bending mode of the hydrocarbon backbone can be sometimes observed (see the green curve in Fig. 3a) but are below or only marginally above the noise threshold in Fig. 2a even at the most positive sample potential. The highest frequency peak is assigned to the C–H stretch of the cyclopentadienyl rings, which was observed in ex situ IRRAS measurements at 3100 cm^{-1} for FcC$_{11}$SH SAMs.[35,36] However, numerous in situ IR studies report the position of this ring mode at ∼10 cm^{-1} higher frequencies.[35,37,38] Ye et al.[36] indicated that the frequency of this band likely depends on the permittivity of the local environment surrounding the Fc center. The frequency of the asymmetric methylene stretching modes at ∼2920 cm^{-1} is known to be highly dependent on the degree of hydrocarbon order in SAMs.[39,40] The asymmetric stretch is observed below 2918 cm^{-1} in a well-ordered, long-chain alkanethiol monolayer.[41] The relatively lower frequency for the asymmetric methylene stretch reported herein may indicate that the FcC$_{11}$SH SAMs formed on the Au islands on ITO may be better ordered than those reported in previous studies on continuous gold films.[35–37] Nevertheless, the potential-dependent ATR-SEIRAS spectra are largely consistent with earlier reports of Fc-containing SAMs. Ye et al.[36]
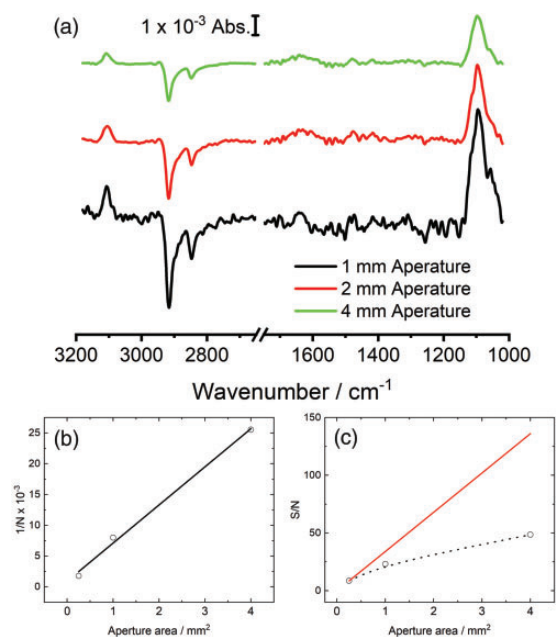
attributed the negative absorbance difference in the methylene stretching units to a potential-dependent reorientation of the hydrocarbon backbone to a more upright position upon oxidation of the redox center. Surface selection rules support this contention, as an upright orientation of the backbone renders the transition dipole moment of both methylene modes increasingly perpendicular to the surface. Viana et al.[38] argued that oxidation leads to a rotation of the ferrocenium center about the bond between the Cp ring and the terminal carbon of the alkyl chain. The rotated Fc$^+$ is aligned with the Cp rings perpendicular to the metal surface, which gives stronger enhancement as per the SEIRAS surface selection rules. Rudnev et al.'s SEIRAS studies[37] indicated that the potential-driven reorientation of both the hydrocarbon chain and the Fc headgroup was operative as shown schematically in Fig. 2b. While the IR spectra in Fig. 2a generally compares favorably to the ATR-SEIRAS reported by Rudnev et al.,[37] one difference is the weaker IR modes of the Cp hydrocarbon vibration compared to the intensities of the methylene vibrations. In that work, FcC$_{11}$SH SAMs prepared on Au surfaces deposited on Si IREs through electron beam deposition showed almost equal peak intensities for C–H ring mode at 3106 cm^{-1} compared to the C–H mode of the alkane backbone of the FcC$_{11}$SH. We obtained similar ATR-SEIRAS when we prepared FcC$_{11}$SH SAMs on continuous gold films directly deposited on Si (data not shown). The relatively weaker signal from the Cp ring when using Au@ITO may be caused by a higher degree of SAM order, which

partially frustrates rotation of the Cp ring upon oxidation of the ferrocene center.

Heterogeneity of ATR-SEIRAS Spectra

One of the appeals of using conductive metal oxide (CMO) films on internal reflection elements for ATR-SEIRAS is the relative ease with which metallic nanoparticles can be either physically deposited or electrodeposited on the surface. This provides a highly accessible means to study nanoparticle-catalyzed reactions with surface sensitive infrared spectroscopy. However, in a previous report, we noted that the density and distribution of electrodeposited metal nanoparticles deposited on CMO-modified IREs are quite variable over the surface.[18] The impact of heterogeneity on ATR-SEIRAS performance can be demonstrated by examining the potential-dependent spectra of $FcC_{11}SH$ SAMs as a function of the spectrometer's built-in Jacquinot-stop (J-stop) aperture as shown in Fig. 3a. Typically, the J-stop is changed to achieve a desired spectral resolution, but it has the secondary effect of changing the size of the beamspot at sample, with larger apertures illuminating larger areas. In a typical ATR-SEIRAS experiment, the J-stop is adjusted to maximize the illuminated area on the working electrode portion of the principal reflecting plane of the IRE. Sacrificing spectral resolution for higher light throughput is desirable for condensed matter measurements from a signal-to-noise (S/N) perspective. This is verified in Fig. 3b, which plots the inverse of the noise level of the ATR-SEIRAS spectra shown in part (a) of the figure as a function of the aperture area. The inverse of the noise level is found to be proportional to the aperture area, which is the expected result when the source overfills the aperture. The slope of the line in Fig. 3b is $k = 6.2 \times 10^3 \, mm^{-2}$. In surface sensitive infrared spectroscopy, where the absorbance is the product of an effective molar absorption coefficient and the surface concentration of adsorbed molecules, the signal should be independent of the aperture area when one assumes a spatially uniform surface enhancement factor. Consequently, a plot of S/N versus aperture area is expected to be linear with a slope equal to the product of the inherent absorbance of the system and k. Using the experimentally measured signal value for the 1 mm aperture (Fig. 3a), the expected dependence of the S/N is plotted in Fig. 3c as the red line. The measured S/N ratios plotted in Fig. 3c are clearly significantly below the expected values for higher apertures and indicate that the surface enhancement factor for the electrodeposited gold islands is not homogeneously distributed across the surface of the IRE.

Mapping the ATR-SEIRAS Response

We recently reported the development of a horizontal ATR microscope end station at the mid-IR beamline at the Canadian Light Source (CLS) that allows for the measurement of ATR spectra with a spot size of $\sim 150 \, \mu m$.[42] We have used this beamline to chemically image H/D isotope exchange processes occurring in microfluidic devices printed directly onto a Si μ-groove IREs.[43] In this study, the endstation was combined with the $FcC_{11}SH$ system in an effort to correlate the spatial distribution of the IR signal with structural heterogeneity on the electrodeposited Au@ITO layers on the Si μ-groove IRE. To facilitate comparison, the exact same modified Si μ-groove IRE used in the conventional spectrometer was transferred to the horizontal microscope. Figure 4a shows a schematic representation of the cross-section of a Si μ-groove IRE under focus at the horizontal microscope, whereas Fig. 4b shows a corresponding plan view. The electroactive surface area, as defined by the Viton O-ring of the spectroelectrochemical cell, is shown as a black circle in Fig. 4b. The Si μ-groove IRE was positioned such that the beam was focused at the origin (black dot in Fig. 4b), chosen to be the position at the approximate center of the wafer, which gave a maximum IR signal. Figure 4c shows the results, at this position, of the potential-dependent FT-IR measurement of the $FcC_{11}SH$ SAM during anodic potential steps from +0.2 V to +0.6 V versus Ag/AgCl. Qualitatively, the spectra are very similar to those obtained on a conventional spectrometer (Fig. 2a). However, a comparison of the S/N of the spectrum at +0.6 V in Fig. 4 with the equivalent spectrum at 1 mm aperture (*viz.* Fig. 2a) is about 50% higher on the horizontal microscope. This demonstrates an appreciable synchrotron advantage caused by the greater geometric étendue of the synchrotron.[42]

A series of mapping measurements were performed by translating the Si μ-groove IRE in the *y*-axis direction (as indicated by the green arrow in Fig. 4b) in 100 μm increments. Figure 5a shows the potential difference spectra for the $FcC_{11}SH$ SAM over a single period of the groove pitch
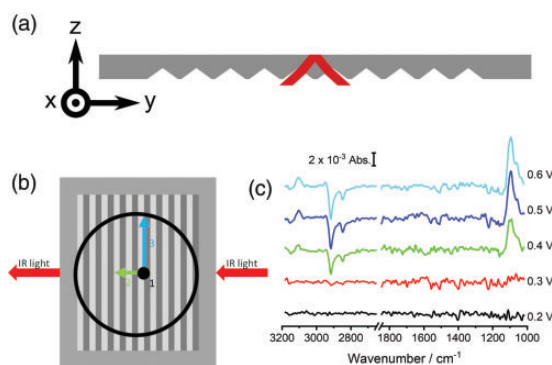

Figure 4. (a) Schematic representation of the Si μ-groove IRE in cross section and (b) as viewed from underneath. (c) Potential-dependent ATR-SEIRAS spectra of $FcC_{11}SH$ measured on the groove at the orign position. Reference spectrum was collected at +0.10 V versus Ag/AgCl.
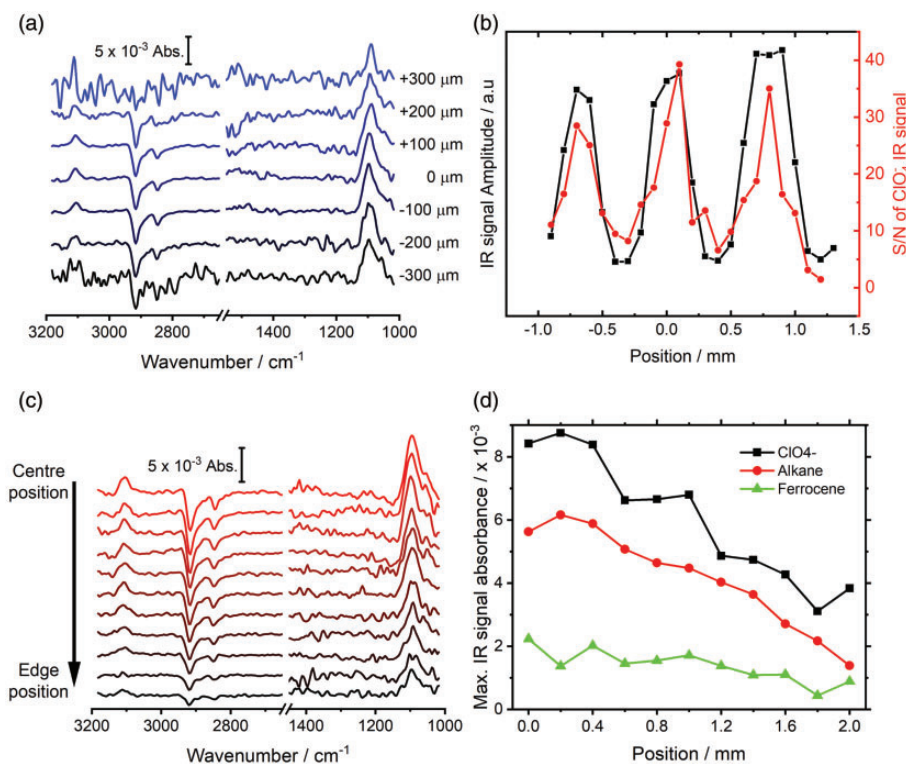
Figure 5. Mapping the heterogeneity of the Au@ITO-modified Si μ-groove IRE using the potential-dependent ATR-SEIRAS spectra of FcC$_{11}$SH. (a) Spectra collected at different positions, as measured from the origin, over the period of a single groove. (b) Correlation between light intensity on the detector (black points) and S/N ratio of the perchlorate peak (red points) over several grooves. (c) Spectra along a single groove moving from the centre position toward the edge position. (d) Signal levels as a function of position along the direction of a single groove.

(∼700 μm). Figure 5b plots the S/N of the perchlorate absorption band and the absolute value of the detector signal as a function of position along the y-axis. The origin of the periodicity in the IR signal amplitude was previously reported[42] and is caused by off-reflection of the incident IR beam, when increasingly misaligned with a groove wall. Severe degradation of the S/N is observed when the beam is offset more than ±200 μm from a position of maximum intensity in the integrated detector amplitude. Nevertheless, the three S/N maxima in Fig. 5b are very similar and indicate that within the 2 mm of travel (centered about the origin) along the y-axis, the quality of the SEIRAS measurements is largely independent of position. It is convenient to map the ATR-SEIRAS response by moving the beam position along one groove face, i.e., along the x-axis (blue arrow in Fig. 4b). Figure 5c shows the IR spectra of FcC$_{11}$SH oxidation at various positions along a single groove, starting from the center of the electroactive area to an edge position. When the IR beam is focused near the center of the of the electrodeposited Au@ITO electrode, the magnitude of the FcC$_{11}$SH IR signals is at their maximum. In fact, the bands have about 30% greater magnitude than those in the spectra collected on the conventional spectrometer using a 1 mm aperture. This highlights the capability of the horizontal microscope to achieve excellent

SEIRAS spectra quality by selectively interrogating a small area of high enhancement. Moving the sampled position towards the edge of the electroactive area over a distance of 2 mm results in a stark decrease in signal strength for all IR modes with a concomitant increase in the noise level. The methylene and Cp C–H stretching modes are barely above the noise at the position furthest from the origin. Figure 5d plots the IR signal of the ring (C–H at 3106 cm^{-1}) and methylene bridge (C–H at 2918 cm^{-1}) hydrocarbon stretching modes as well as the ClO$_4^-$ anions (1096 cm^{-1}) with their corresponding position along the groove of the Si μ-groove IRE. The result clearly highlights significant heterogeneity in SEIRAS response, as each of the IR modes experience a reduction in signal amplitude of more than 50%.

Origin of the Heterogeneity in the ATR-SEIRAS Response

The data above clearly indicate that the quality of the ATR-SEIRAS spectra significantly depends on the area of the Au@ITO substrate being irradiated. However, it is unclear whether the spectral changes in the FcC$_{11}$SH spectra are related to heterogeneity in the SAM coverage, the SEIRAS activity of the electrodeposited Au@ITO, or a combination of both. To investigate the origin of the heterogeneity, SEM
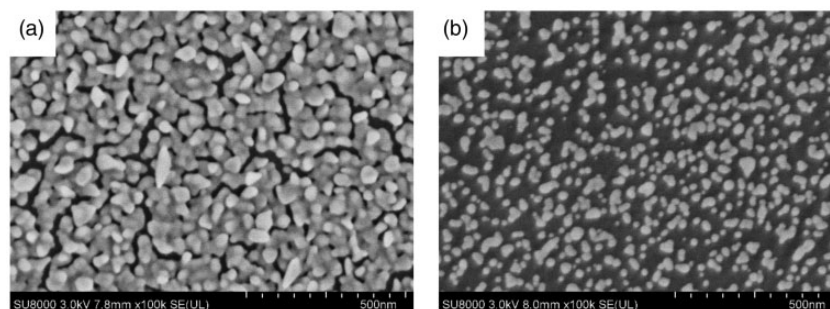
Figure 6. SEM images of Au island films electrodeposited on ITO-modified Si μ-groove IRE (a) near the middle of the electroactive area and (b) closer to the periphery.

images in Fig. 6 show the Au@ITO surface at the center of the (a) electrode area and (b) towards the edge. Based on image analysis, the electrodeposited Au coverage on ITO can vary from a 91% coverage at the center to only 34% coverage at the edge.

The electrodeposited Au layers change from an almost continuous layer of Au with some multilayer features in Fig. 6a to sparse individual grains with a mean grain size of ∼500 nm in Fig. 6b. The SEM images demonstrate that the variable Au nanoparticle density is the likely source of the pronounced differences in the IR signal in the SEIRAS measurements. The trivial explanation is that the lower gold nanoparticle density on the periphery of the working electrode leads to a corresponding lower surface concentration of $FcC_{11}SH$ molecules in the beamspot. However, this simple explanation is likely incomplete as the SEM image analysis would predict an approximate three-fold lower thiol concentration as opposed to the two-fold decrease in signal as per Fig. 5. Surface enhancement factors are known to be dependent on grain size and structure of the metal layer,[44] making it likely that the more percolated gold layer in Fig. 6a has a fundamentally lower enhancement factor than the more discrete gold nanoparticles found further from the center of the electroactive area. In principle, effective medium theories can model the enhancement factors of different packing metallic particles densities.[18,44–46] However, they generally only provide results that qualitatively match experimental results due to the required oversimplification of the nanoparticle geometry. Improvements in optical modeling, or the use of more precisely geometrically defined nanoparticles, would be of great value in differentiating the roles of effective SAM surface concentration from the fundamental differences in enhancement factors arising from different metallic film densities.

Conclusion

The self-assembly of a redox-active monolayer of a ferrocene thiol molecule has been studied using ATR-SEIRAS. The potential-dependent redox behavior of the ferrocene

SAM in an IR spectroelectrochemical cell was found to be in very good agreement with the known propensity of this system to give kinetic and thermodynamic dispersion. Applying potentials that oxidize the ferrocene headgroup lead to strong changes in the IR response, consistent with the ingress of perchlorate counterions and both a reorientation of the alkyl chain backbone and a rotation about the C–Cp bond. The potential-dependent changes have provided a convenient system to study heterogeneity in SEIRAS active films formed through the electrodeposition of gold nanoparticle islands. The consequence of the distributed nanoparticle density was only observed on a conventional spectrometer equipped with a conventional ATR-SEIRAS optical arrangement by changing the J-stop aperture. Transferring the sample to a horizontal ATR microscope and using SIR radiation allowed the heterogeneity to be mapped in two orthogonal line scans. The ability to select a smaller area of the SEIRAS substrate using the horizontal ATR microscope endstation leads to a factor of two improvement in the absorbance magnitude. Although the geometrical fill factor of the electrodeposited gold provides a simple explanation of the higher signals obtained from certain regions of the surface, a nanoparticle density-dependent contribution to the intrinsic enhancement factor is also operative. The current work demonstrates that the horizontal ATR microscope, when combined with SIR, is a powerful tool to study spatially distributed heterogeneity in (electro)chemical reactions. We are currently working to improve the de-magnification factor of an imaging detector (e.g., focal plane array) installed on the horizontal ATR microscope.[43] Once these improvements are realized, the instrument will provide nearly an order of magnitude better spatial resolution. We envision that such a tool will be highly valuable in assessing heterogeneity in catalyst layers under in situ or operando electrochemical conditions.

Declaration of Conflicting Interests

The author(s) declared no potential conflicts of interest with respect to the research, authorship, and/or publication of this article.

Funding

ORCID iDs

Scott M. Rosendahl https://orcid.org/0000-0003-1471-0241
Ian J. Burgess https://orcid.org/0000-0001-9611-1431

References

1. R. Schlögl. "Heterogeneous Catalysis". Angew. Chem. Int. Ed. 2015. 54(11): 3465–3520.
2. M.J.S. Farias, J.M. Feliu. "Determination of Specific Electrocatalytic Sites in the Oxidation of Small Molecules on Crystalline Metal Surfaces". Top. Curr. Chem. 2019. 377(1): 5.
3. D. Bizzotto, I.J. Burgess, T. Doneux, et al. "Beyond Simple Cartoons: Challenges in Characterizing Electrochemical Biosensor Interfaces". ACS Sens. 2018. 3(1): 5–12.
4. A. Schneider, L. Colmenares, Y.E. Seidel, Z. Jusys, et al. "Transport Effects in the Oxygen Reduction Reaction on Nanostructured, Planar Glassy Carbon Supported Pt/GC Model Electrodes". Phys. Chem. Chem. Phys. 2008. 10(14): 1931–1943.
5. G.V. Fortunato, E. Pizzutilo, A.M. Mingers, O. Kasian, et al. "Impact of Palladium Loading and Interparticle Distance on the Selectivity for the Oxygen Reduction Reaction Toward Hydrogen Peroxide". J. Phys. Chem. C. 2018. 122(28): 15878–15885.
6. H. Mistry, F. Behafarid, R. Reske, A.S. Varela, et al. "Tuning Catalytic Selectivity at the Mesoscale via Interparticle Interactions". ACS Catal. 2016. 6(2): 1075–1080.
7. O.Q. Carvalho, P. Adiga, S.K. Murthy, J.L. Fulton, et al. "Understanding the Role of Surface Heterogeneities in Electrosynthesis Reactions". iScience. 2020. 23(12): 101814.
8. M. Osawa. "In-Situ Surface-Enhanced Infrared Spectroscopy of the Electrode/Solution Interface". In: A.C. Alkire, D.M. Kolb, J. Lipkowski, P.N. Ross, editors. Advances in Electrochemical Science and Engineering. New York: Wiley-VCH, 2008. Chap. 8, Pp. 269–314.
9. X.-Y. Ma, C. Ding, H. Li, K. Jiang, et al. "Revisiting the Acetaldehyde Oxidation Reaction on a Pt Electrode by High-Sensitivity and Wide-Frequency Infrared Spectroscopy". J. Phys. Chem. Lett. 2020. 11(20): 8727–8734.
10. C. Zhu, B. Lan, R.-L. Wei, et al. "Potential-Dependent Selectivity of Ethanol Complete Oxidation on Rh Electrode in Alkaline Media: A Synergistic Study of Electrochemical ATR SEIRAS and IRAS". ACS Catal. 2019. 9(5): 4046–4053.
11. K. Jiang, J.-Y. Wang, T.-T. Zhao, W.-B. Cai. "Formic Acid Oxidation at Palladium Electrode in Acidic Media Containing Chloride Anions: An In Situ ATR SEIRAS Investigation". J. Electroanal. Chem. 2017. 800: 77–81.
12. M. Hiroto, O. Masatoshi. "Surface-Enhanced Infrared Spectrum of CO Adsorbed on Cu Electrodes in Solution". Chem. Lett. 2004. 33(3): 278–279.
13. S.-J. Huo, X.-K. Xue, Q.-X. Li, et al. "Extending in Situ Attenuated-Total-Reflection Surface-Enhanced Infrared Absorption Spectroscopy to Ni Electrodes". J. Phys. Chem. B. 2006. 110(9): 4162–4169.
14. Y.-H. Lu, J.M. Larson, A. Baskin, X. Zhao, et al. "Infrared Nanospectroscopy at the Graphene–Electrolyte Interface". Nano Lett. 2019. 19(8): 5388–5393.
15. E. Strelcov, C. Arble, H. Guo, B.D. Hoskins, et al. "Nanoscale Mapping of the Double Layer Potential at the Graphene–Electrolyte Interface". Nano Lett. 2020. 20(2): 1336–1344.
16. M.J. Lardner, K. Tu, S.M. Rosendahl, et al. "Spatiotemporal Mapping of Diffusion Layers Using Synchrotron Infrared Radiation". Electrochim. Acta. 2015. 162: 72–78.
17. K. Tu, M.J. Lardner, T.A. Morhart, S.M. Rosendahl, et al. "Spatial Mapping of Methanol Oxidation Activity on a Monolithic Variable-Composition PtNi Alloy Using Synchrotron Infrared Microspectroscopy". J. Phys. Chem. C. 2016. 120(41): 23640–23647.
18. I.R. Andvaag, T.A. Morhart, O.J.R. Clarke, I.J. Burgess. "Hybrid Gold–Conductive Metal Oxide Films for Attenuated Total Reflectance Surface Enhanced Infrared Absorption Spectroscopy". ACS Appl. Nano Mater. 2019. 2(3): 1274–1284.
19. Y. Feng, E.R. Dionne, V. Toader, et al. "Odd–Even Effects in Electroactive Self-Assembled Monolayers Investigated by Electrochemical Surface Plasmon Resonance and Impedance Spectroscopy". J. Phys. Chem. C. 2017. 121(44): 24626–24640.
20. A.J. Steckl, G. Mohammed. "The Effect of Ambient Atmosphere in the Annealing of Indium Tin Oxide Films". J. Appl. Phys. 1980. 51(7): 3890–3895.
21. S.R. Smith, S. Han, A. McDonald, et al. "An Electrochemical Approach to Fabricate a Heterogeneous Mixed Monolayer on Planar Polycrystalline Au and its Characterization with Lateral Force Microscopy". J. Electroanal. Chem. 2012. 666: 76–84.
22. C.A. Widrig, C. Chung, M.D. Porter. "The Electrochemical Desorption of n-Alkanethiol Monolayers from Polycrystalline Au and Ag Electrodes". J. Electroanal. Chem. Interfacial Electrochem. 1991. 310(1): 335–359.
23. L.Y.S. Lee, T.C. Sutherland, S. Rucareanu, R.B. Lennox. "Ferrocenylalkylthiolates as a Probe of Heterogeneity in Binary Self-Assembled Monolayers on Gold". Langmuir. 2006. 22(9): 4438–4444.
24. H. Tian, Y. Dai, H. Shao, H.-Z. Yu. "Modulated Intermolecular Interactions in Ferrocenylalkanethiolate Self-Assembled Monolayers on Gold". J. Phys. Chem. C. 2013. 117(2): 1006–1012.
25. A.J. Bard, L.R. Faulkner. "Electroactive Layers and Modified Electrodes". Electrochemical Methods: Fundamentals and Applications. New York: John Wiley and Sons, Inc., 2000. Chap. 14, Pp. 580–631.
26. N. Nerngchamnong, D. Thompson, L. Cao, L. Yuan, et al. "Nonideal Electrochemical Behavior of Ferrocenyl–Alkanethiolate SAMs Maps the Microenvironment of the Redox Unit". J. Phys. Chem. C. 2015. 119(38): 21978–21991.
27. R.A. Wong, Y. Yokota, M. Wakisaka, et al. "Discerning the Redox-Dependent Electronic and Interfacial Structures in Electroactive Self-Assembled Monolayers". J. Am. Chem. Soc. 2018. 140(42): 13672–13679.

28. K. Uosaki, Y. Sato, H. Kita. "Electrochemical Characteristics of a Gold Electrode Modified with a Self-Assembled Monolayer of Ferrocenylalkanethiols". Langmuir. 1991. 7(7): 1510–1514.

29. R.C. Chambers, C.E. Inman, J.E. Hutchison. "Electrochemical Detection of Nanoscale Phase Separation in Binary Self-Assembled Monolayers". Langmuir. 2005. 21(10): 4615–4621.

30. J.J. Calvente, R. Andreu, M. Molero, et al. "Influence of Spatial Redox Distribution on the Electrochemical Behavior of Electroactive Self-Assembled Monolayers". J. Phys. Chem. B. 2001. 105(39): 9557–9568.

31. C.E.D. Chidsey, C.R. Bertozzi, T.M. Putvinski, A.M. Mujsce. "Coadsorption of Ferrocene-Terminated and Unsubstituted Alkanethiols on Gold: Electroactive Self-Assembled Monolayers". J. Am. Chem. Soc. 1990. 112(11): 4301–4306.

32. T. Auletta, F.C.J.M. van Veggel, D.N. Reinhoudt. "Self-Assembled Monolayers on Gold of Ferrocene-Terminated Thiols and Hydroxyalkanethiols". Langmuir. 2002. 18(4): 1288–1293.

33. J.A. Sigrist, E.S. Lins, T.A. Morhart, et al. "Optimization of a Commercial Variable Angle Accessory for Entry Level Users of Electrochemical Attenuated Total Reflection Surface-Enhanced Infrared Absorption Spectroscopy (ATR SEIRAS)". Appl. Spectrosc. 2019. 73(12): 1394–1402.

34. U.E. Zhumaev, A.S. Lai, I.V. Pobelov, A. Kuzume, et al. "Quantifying Perchlorate Adsorption on Au(111) Electrodes". Electrochim. Acta. 2014. 146: 112–118.

35. D.D. Popenoe, R.S. Deinhammer, M.D. Porter. "Infrared Spectroelectrochemical Characterization of Ferrocene-Terminated Alkanethiolate Monolayers at Gold". Langmuir. 1992. 8(10): 2521–2530.

36. S. Ye, Y. Sato, K. Uosaki. "Redox-Induced Orientation Change of a Self-Assembled Monolayer of 11-Ferrocenyl-1-undecanethiol on a Gold Electrode Studied by In Situ FT-IRRAS". Langmuir. 1997. 13(12): 3157–3161.

37. A.V. Rudnev, U. Zhumaev, T. Utsunomiya, C. Fan, et al. "Ferrocene-Terminated Alkanethiol Self-Assembled Monolayers: An Electrochemical and In Situ Surface-Enhanced Infra-Red Absorption Spectroscopy Study". Electrochim. Acta. 2013. 107: 33–44.

38. A.S. Viana, A.H. Jones, L.M. Abrantes, M. Kalaji. "Redox Induced Orientational Changes in a Series of Short Chain Ferrocenyl Alkyl Thiols Self-Assembled on Gold(111) Electrodes". J. Electroanal. Chem. 2001. 500(1): 290–298.

39. L. Bertilsson, B. Liedberg. "Infrared Study of Thiol Monolayer Assemblies on Gold: Preparation, Characterization, and Functionalization of Mixed Monolayers". Langmuir. 1993. 9(1): 141–149.

40. M.D. Porter, T.B. Bright, D.L. Allara, C.E.D. Chidsey. "Spontaneously Organized Molecular Assemblies. 4. Structural Characterization of n-Alkyl Thiol Monolayers on Gold by Optical Ellipsometry, Infrared Spectroscopy, and Electrochemistry". J. Am. Chem. Soc. 1987. 109(12): 3559–3568.

41. F. Bensebaa, T.H. Ellis, A. Badia, R.B. Lennox. "Thermal Treatment of n-Alkanethiolate Monolayers on Gold, as Observed by Infrared Spectroscopy". Langmuir. 1998. 14(9): 2361–2367.

42. T.A. Morhart, S. Read, G. Wells, M. Jacobs, et al. "Attenuated Total Reflection Fourier Transform Infrared (ATR FT-IR) Spectromicroscopy Using Synchrotron Radiation and Micromachined Silicon Wafers for Microfluidic Applications". Appl. Spectrosc. 2018. 72(12): 1781–1789.

43. T.A. Morhart, S.T. Read, G. Wells, M. Jacobs, et al. "Micromachined Multigroove Silicon ATR FT-IR Internal Reflection Elements for Chemical Imaging of Microfluidic Devices". Anal. Methods. 2019. 11(45): 5776–5783.

44. A.E. Bjerke, P.R. Griffiths, W. Theiss. "Surface-Enhanced Infrared Absorption of CO on Platinized Platinum". Anal. Chem. 1999. 71(10): 1967–1974.

45. M. Osawa, K.-I. Ataka, K. Yoshii, T. Yotsuyanagi. "Surface-Enhanced Infrared ATR Spectroscopy for In Situ Studies of Electrode/Electrolyte Interfaces". J. Electron Spectrosc. Relat. Phenom. 1993. 64–65: 371–379.

46. C. Pecharromán, A. Cuesta, C. Gutiérrez. "Comments on the Paper by M.-S. Zheng and S.-G. Sun Entitled 'In Situ FT-IR Spectroscopic Studies of CO Adsorption on Electrodes with Nanometer-scale Thin Films of Ruthenium in Sulfuric Acid Solutions' [J. Electroanal. Chem. 500 (2001) 223]". J. Electroanal. Chem. 2002. 529(2): 145–154.